Evaluation of different methods of determining the angle of attack on wind turbine blades under yawed inflow conditions

Vimalakanthan, K.; Schepers, J. G.; Shen, W. Z.; Rahimi, H.; Micallef, D.; Simao Ferreira, C. J.; Jost, E.; Klein, L.

DOI
10.1088/1742-6596/1037/2/022028

Publication date
2018

Document Version
Final published version

Published in
Journal of Physics: Conference Series

Towards improving the aerodynamic performance of a ducted wind turbine: A numerical study

IOP Conf. Series: Journal of Physics: Conf. Series **1037** (2018) 022016 doi:10.1088/1742-6596/1037/2/022016

Towards improving the aerodynamic performance of a ducted wind turbine: A numerical study

V.V. Dighe, G. de Oliveira, F. Avallone, G.J.W. van Bussel

Wind Energy Research Group, Delft University of Technology, Delft, Netherlands, 2629HS

E-mail: V.V.Dighe@tudelft.nl

Abstract. This paper aims to study the aerodynamic performance of ducted wind turbines (DWT) using inviscid and viscous flow calculations by accounting for the mutual interaction between the duct and the rotor. Two generalized duct cross section geometries are considered while the rotor is modelled as an actuator disc with constant thrust coefficient. The analysis shows the opportunity to significantly increase the overall aerodynamic performance of the DWT by a correct choice of the optimal rotor loading for a given duct geometry. Present results clearly indicate that the increased duct cross section camber leads to an improved performance for a DWT. Finally, some insights on the changes occurring to the performance coefficients are obtained through a detailed flow analysis.

1. Introduction

Ducted wind turbines (DWT) have been developed to improve the power extraction, in comparison to a bare turbine, by increasing the mass flow through the rotor. A significant amount of literature on DWT investigations is based on the combined use of theoretical, numerical and experimental techniques [1, 2, 3, 4, 5, 6]. Owing to the low computational costs, it clearly appears that the classical axial momentum theory (AMT) still remains popular for the analysis of DWT. In the last years, a significant body of literature dealing with this topic has been proposed [7, 8, 9]. The main limitation of the AMT approach is that the mutual interaction between the duct and the rotor is neglected. This means that a linear relation between the axial force exerted by the duct and the rotor on the fluid, or vice-versa, is implicitly assumed. As a consequence the optimal rotor loading coefficient corresponds to 8/9 despite the presence of the duct. In comparison, the higher order CFD techniques naturally account for the nonlinear mutual interaction between the duct and the rotor. Introducing an actuator disc (AD) model in a CFD based method allows a good representation of flow past the rotor. Using the AD approach, Hjort and Larsen [10] carried out a comprehensive study on the existing DWT designs using AMT, inviscid and RANS calculations. They found that the gain in the power extraction, when employing a multi-layer duct-design with passive boundary-layer stall control, exceeds by 50% compared to any horizontal axis wind turbine (HAWT) or DWT bearing the same rotor diameter. In addition, the paper also discusses the upper limits of power extraction for specific DWT designs, similar to the Betz limit applicable for bare HAWT. More recently, Bontempo and Manna studied the effects of the duct cross section camber on the performance of DWT using a semi-analytical AD method [11]. The model, characterized by a low computational cost, shows good agreement with the higher order RANS approach. They investigated the performance

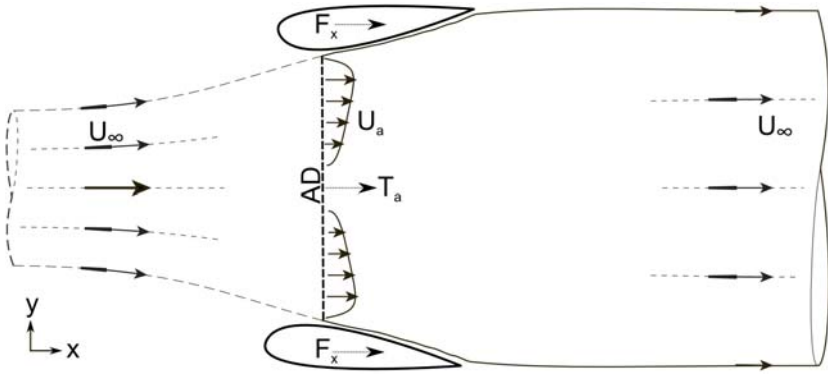

Figure 1. Schematic of duct-actuator flow model. Inflow is assumed far upstream and outflow is assumed far downstream in a fully developed wake.

of DWT adopting a generalized duct shape with variable camber. In their investigation, the duct camber was varied by bending the rear part of the duct profile in the outward direction by 5 and 10 degrees. In this way, the effective duct rotor to exit area ratio was also varied, and therefore the performance improvement attributed to the change of the duct camber only, creates confusion when the power coefficient is calculated using the duct exit section. Moreover, the aerodynamic interaction principle between a duct and the rotor for a DWT lacks clarity, and therefore the topic of the current discussion.

The present paper aims to extend the formative work of de Oliveira et al. [12] for studying the conservative force interaction mechanisms between an axisymmetric body and an AD. One of the conclusions of de Oliveira et al. [12] study was that the force interaction mechanisms between a body and an AD generally affect the actuator loading at which the optimal power coefficient is reached. The present contribution is an attempt to verify this claim through CFD by evaluating the performance of the duct-actuator model; an analogy that relates the duct with the axisymmetric body.

Section 2 of this article discusses the governing performance coefficients for a duct-actuator model estimated from the numerical predictions. The numerical methods used consists of a panel method and RANS CFD, briefly described in section 3. Finally some insights on the trend of these performance coefficients with respect to AD loading and the duct thrust will be discussed in section 4, together with flow analysis obtained using RANS simulations.

2. Performance of duct-actuator flow model

Based on the existing literature and previous validation studies conducted by the authors [13, 14], the incompressible flow past a turbine is modelled by a flat AD of infinitesimal width, Figure 1. The AD exerts a constant thrust force T_a per unit surface, which corresponds to a non-dimensional thrust force coefficient:

$$C_T = \frac{T_a}{\frac{1}{2}\rho U_\infty^2 S_a}, \tag{1}$$

where ρ is the fluid density, U_∞ is the free stream velocity and S_a is the AD surface area.

For a duct-actuator configuration, an additional induced drag force F_x, exerted by the duct on the flow, appears. In order to quantify the relative contribution of the duct force F_x on the flow-field, the duct force coefficient C_x is defined:

$$C_x = \frac{F_x}{\frac{1}{2}\rho U_\infty^2 S_d}. \tag{2}$$

The computation of the integral of the force term F_x across the duct surface involves several intermediate steps that are regarded outside the scope of the present contribution.

The presence of duct force F_x results in an additional mass flow rate $\dot{\mathbf{m}} = \rho S_a U_a$, when calculated across the AD plane. Although the assumption of constant loading C_T is employed, the free stream velocity computed at the AD plane cannot be regarded as radially uniform; especially for a duct-actuator model where the accelerations are higher as compared to a bare AD. Therefore, the mean AD velocity U_a is defined by integrating the free stream velocity components across the actuator surface:

$$U_a = \frac{1}{S_a} \int_{rad} U_x dS, \tag{3}$$

where U_x is the differential axial velocity term across the AD surface dS in the free stream direction x.

This leads to a power coefficient of the duct-actuator model using actuator surface S_a as the reference area:

$$C_P = \frac{P}{\frac{1}{2}\rho U_\infty^3 S_a} = \frac{U_a}{U_\infty} C_T. \tag{4}$$

The velocity at the AD U_a and the duct force coefficient C_x are obtained by post-processing the numerical solutions. U_a is then combined with the respective AD loading C_T leading to the power coefficient C_P of the duct-actuator model as in equation (4).

3. Numerical methods

In this section the algorithms and discretization details of the computational codes used will be briefly described. For an in-depth description, the reader can refer to [12, 13]. For all calculations, the characteristic length is normalized with the duct chord length c. The AD measures y/c = 1.0, and placed at the nozzle location of the duct. The tip clearance between the AD tip and the duct nozzle surface is 2.0%c.

3.1. Panel method

A two dimensional potential flow panel method has been used to model the steady isentropic incompressible flow field around a duct-actuator model (see Figure 2) following the work of de Oliviera et al. [12]. The governing equations are simple form of the Euler equations and therefore inviscid. The AD is represented as a non-conservative force term in the vorticity equation. The duct surface is defined using distribution of vortex panels with the local slope such as to reproduce the correct shape. 140 control points are taken around the duct profile in the clockwise direction. In essence, a uniform distribution of vorticity on the duct panels is assigned by assuming the Kutta condition. The simplified assumption of uniform vorticity distribution over the panels represents a simplification of real physics and prevents separation from occurring on the duct surface even for larger pressure gradients. The streamwise discretization is non-uniform, with initial panel length equal to 1.0% of the duct chord length c just behind the AD, and increasing gradually in length as the wake expansion settles further downstream. The panel method, in any case, should be considered to be a successor of the one dimensional models and other similar analysis of DWT. The panel method is particularly appealing for repeated analysis design arrangements due to its short execution time.

3.2. RANS CFD

A commercial CFD solver ANSYS Fluent® has been used for a complete viscous solution of steady incompressible flow around a duct-actuator model represented in Figure 3. The analysis

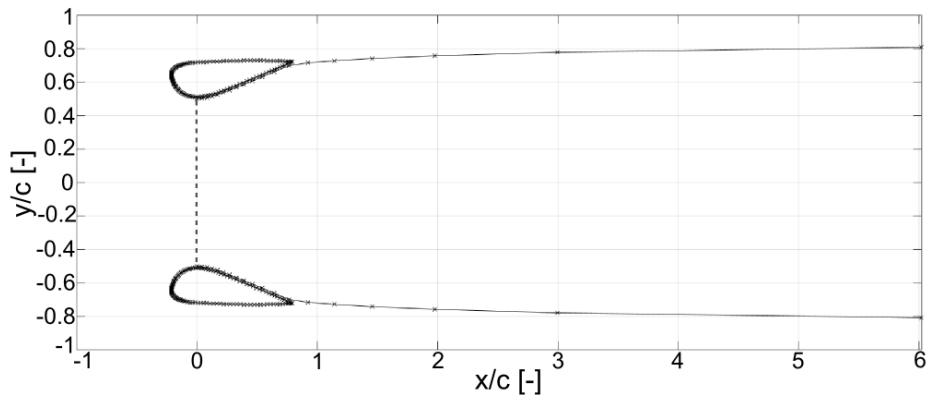

Figure 2. A typical streamline solution obtained using the vortex panel method showing panel distribution along the duct surface and the wake region for the duct-actuator flow model.

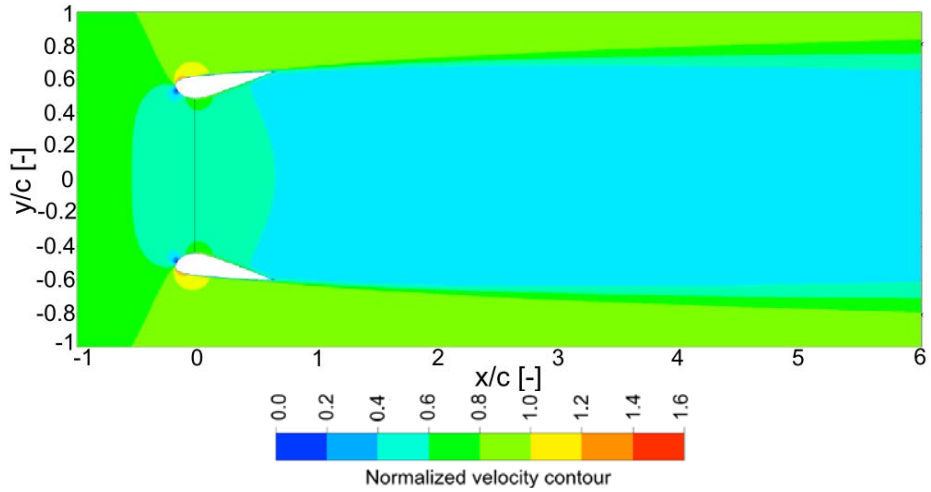

Figure 3. A typical flow field solution obtained using the RANS CFD colored with velocity contours for the duct-actuator flow model.

is again made two dimensional using the AD approach. For detailed numerical setup, see [13]. The governing flow equations are the Reynolds Averaged Navier Stokes equations in planar coordinates. The k-ω SST (shear stress transport) is used as the turbulence model. Preliminary investigations show good agreement with the experiments [13]. The possible pitfalls introduced through the use of turbulence models (instead of resolving turbulence in space and time) and different numerical schemes are well known, however, these errors are minimized by a mesh-independence study [15]. The RANS solution was obtained using the coupled algorithm; it offers robustness and faster convergence for steady state flows as compared to the segregated solution schemes. A least-squares cell-based method is used to evaluate the pressure gradient, with pressure and momentum equations solved using a second order upwind differential scheme. The convergence criteria is set to 10^{-6} for all the residuals. A typical converged RANS solution (single duct-actuator configuration) with approximately 0.1 million mesh elements is obtained in roughly 0.5 hour on a multi-core work-station desktop computer.

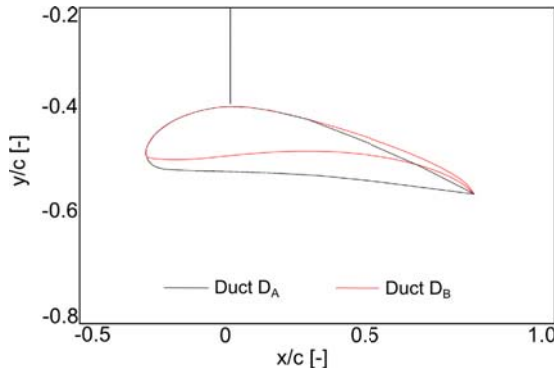

Figure 4. Duct geometry profiles used for the numerical study.

4. Results and discussion

This section investigates the effect of the duct geometry on the performance coefficients of the duct-actuator model by comparing the results of the panel method alongside the results of RANS CFD, as in subsection 4.1. To this aim, two duct geometries D_A and D_B are adopted bearing different cross-section camber, see Figure 4, to highlight the effects of duct profile camber on the performance of the duct-actuator model. The airfoil coordinates represent the DonQi® and the Selig S1223 profiles inclined at an angle of 8 degree with respect to the free stream flow. The chosen angle is in accordance with the commercial DonQi® duct model design. As stressed in the introduction, a constant rotor (nozzle) to outlet area ratio is deliberately imposed, in order to exclude the theoretical debate on the power coefficient definition in which the reference area is taken at the duct exit section. Finally, some insights on the trend of the performance coefficients for variable AD loading and duct geometry are obtained through a close inspection of the flow field in subsection 4.2.

4.1. Performance of duct-actuator model

Figures 5 and 6 shows the results of the numerical simulations for the duct-actuator model, for duct geometries D_A and D_B respectively. The validity range of AMT for the AD loading ($0 \leq C_T \leq 0.9$) is investigated.

Figures 5(a) and 6(a) depicts the correlation between the duct force coefficient C_x and the AD force coefficient C_T obtained for the duct-actuator model for both geometries. The relation between force coefficients (C_x and C_T) is nearly linear at lower AD loadings. Departures from linearity is noticeable at higher AD loadings, with peaks appearing at $C_T \approx 0.6$ and 0.8 for D_A and D_B respectively. In fact, the value of C_x decreases for AD loadings beyond the local maxima. Furthermore, comparing the magnitude of C_x between ducts D_A and D_B, it is evident that the magnitude of C_x increases with the duct profile camber.

Figures 5(b) and 6(b) show the effect of the presence of the ducts D_A and D_B respectively on the normalized axial velocity U_a/U_∞ at AD. For the sake of completeness, U_a/U_∞ for the bare AD is also included to provide insights on the effect of ducts on the flow augmentation. It clearly appears that the duct increases U_a/U_∞, when compared to the bare actuator, for both ducts. Turning now to the comparison between ducts D_A and D_B, it is visible that the duct profile with higher camber, attains a greater U_a/U_∞ resulting in the additional mass flow rate $\dot{\mathbf{m}} = \rho S_a U_a$ drawn across the AD.

Figures 5(c) and 6(c) represents the power coefficients C_P of the bare and ducted actuator (D_A and D_B respectively) as a function of variable AD loading C_T. It is evident that, for the entire range of AD loading C_T, the ducted actuator is characterized by a higher C_P. Present results show that the maximum C_P is obtained for a C_T value, which is lower than 8/9; the maximum

C_P corresponds to $C_T \approx 0.75$ and 0.80 for D_A and D_B respectively. Moreover, increasing the camber of the duct affects the C_T value, which is higher, for maximizing the C_P.

Differences appear between the RANS and the panel method solutions. These discrepancies, highlighted by the under-prediction of the panel method, can be explained as follows. Firstly, the panel method assumes a constant circulation in conjunction with the Kutta condition, as also reported by Hjort and Larsen [10]. Secondly, the inviscid duct wall boundary condition inherently imposed in the panel method eliminates the effect of turbulent mixing occurring usually aft of the AD position. The mixing process will tend to energize the boundary layer flow at the duct walls, especially for thick and cambered airfoils. Nevertheless, the trends for both RANS CFD and panel method solutions match within the tolerable range, and thus considered acceptable.

4.2. Flow field analysis

The performance of the duct-actuator model highlighted in subsection 4.1 is determined by the aerodynamic interactions between the duct and the AD. In order to further understand the effects of the duct geometry and variable AD loading on the global performance coefficients, a flow field analysis using RANS solutions is carried out. Velocity contours colored with normalized free stream velocity $\frac{U}{U_\infty}$ are shown in Figure 7. Contours are plotted on a plane close to the surface of the duct thus allowing a better interpretation of the flow field associated with duct-actuator interactions. In this study, four actuator loadings (C_T = 0.6, 0.7, 0.8 and 0.9) are considered to highlight the non-linear part in the performance trend-lines, as in Figures 5(c) and 6(c). Focusing on Figure 7, and more precisely observing from top to bottom, it can be noticed that the stagnation point moves towards the suction side of the duct with the increasing value of C_T, for both D_A and D_B. Once the stagnation point starts to move towards the suction side of the duct, the velocity magnitude at the AD gradually reduces. Consequently, the magnitude of velocity at the pressure side of the duct starts to increase significantly. Evidence of this can also be highlighted from D_A, $C_T = 0.8$ and D_B, $C_T = 0.9$ in Figure 7. This flow phenomenon, occurring due to the displacement of stagnation point along the surface of the duct, explains the reduction of C_x as in Figures 5(a) and 6(a). The reduction of C_x characterized by reduced velocity $\frac{U}{U_\infty}$ flowing across the AD, leads to reduced C_P at higher actuator loadings C_T, for D_A and D_B.

5. Conclusions

The present article reignites the insight of de Oliveira [12] and contribute to the verification of the study into DWT investigations. In this manuscript, a two-dimensional vortex panel method and RANS CFD are used to investigate the local and global features of the flow. Based on the numerical predictions, the aerodynamic interactions between a duct and an AD:

- is nonlinear and divergence from linearity occurs at higher AD loadings.
- depend on the distinct shape of the duct under consideration.
- affects the optimal AD loading coefficient at which the overall performance is maximized.

Acknowledgments

The research is supported by STW organization, grant number- 12728.

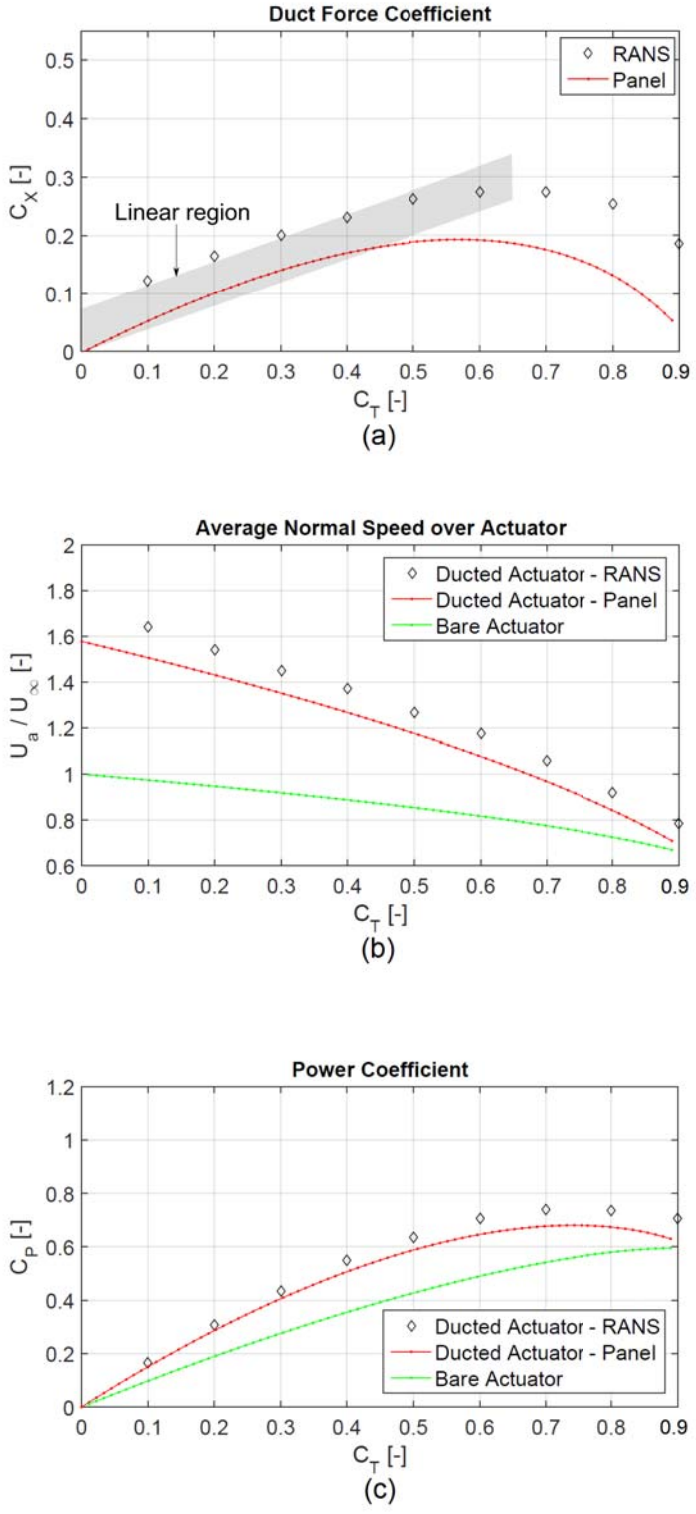

Figure 5. Effect of variable actuator loading on (a) duct force coefficient (b) streamwise normalized velocity at the AD and (c) power coefficient for duct D_A.

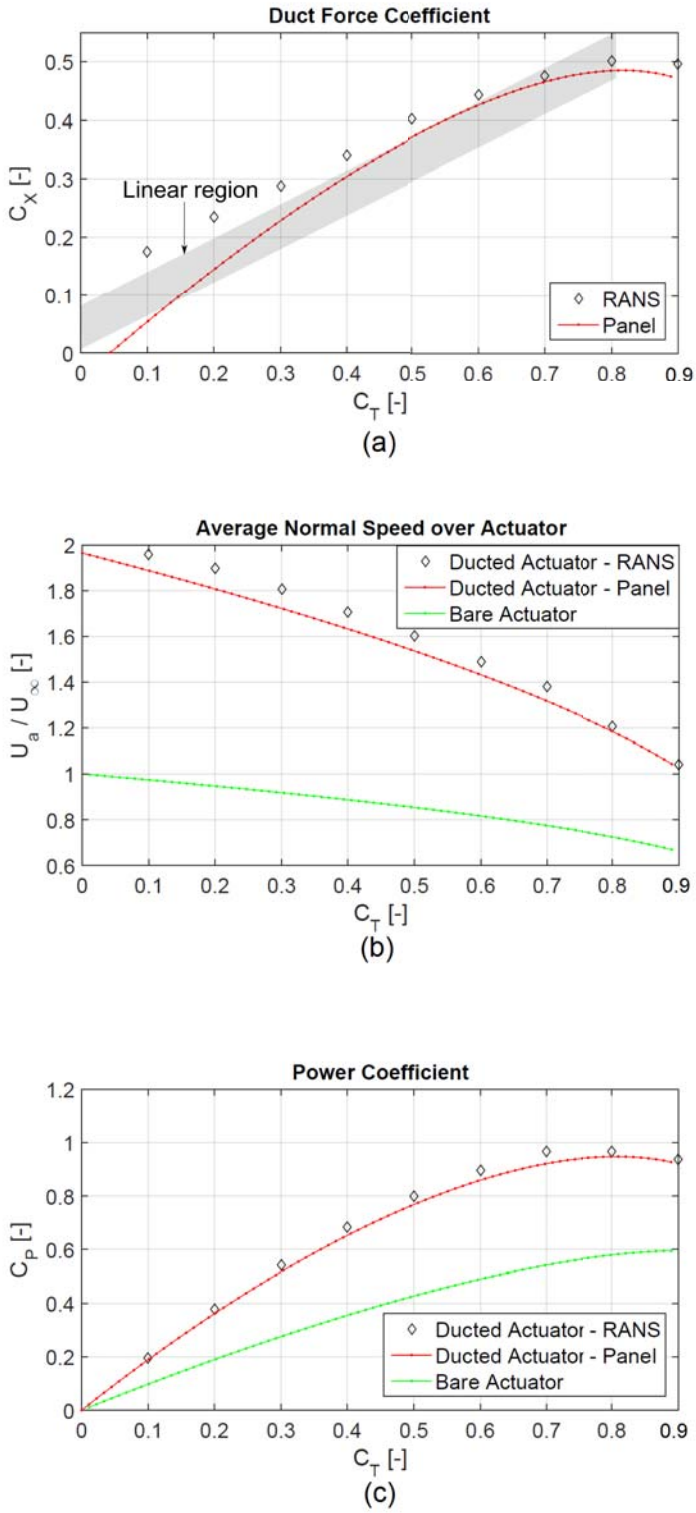

Figure 6. Effect of variable actuator loading on (a) duct force coefficient (b) streamwise normalized velocity at the AD and (c) power coefficient for duct D_B.

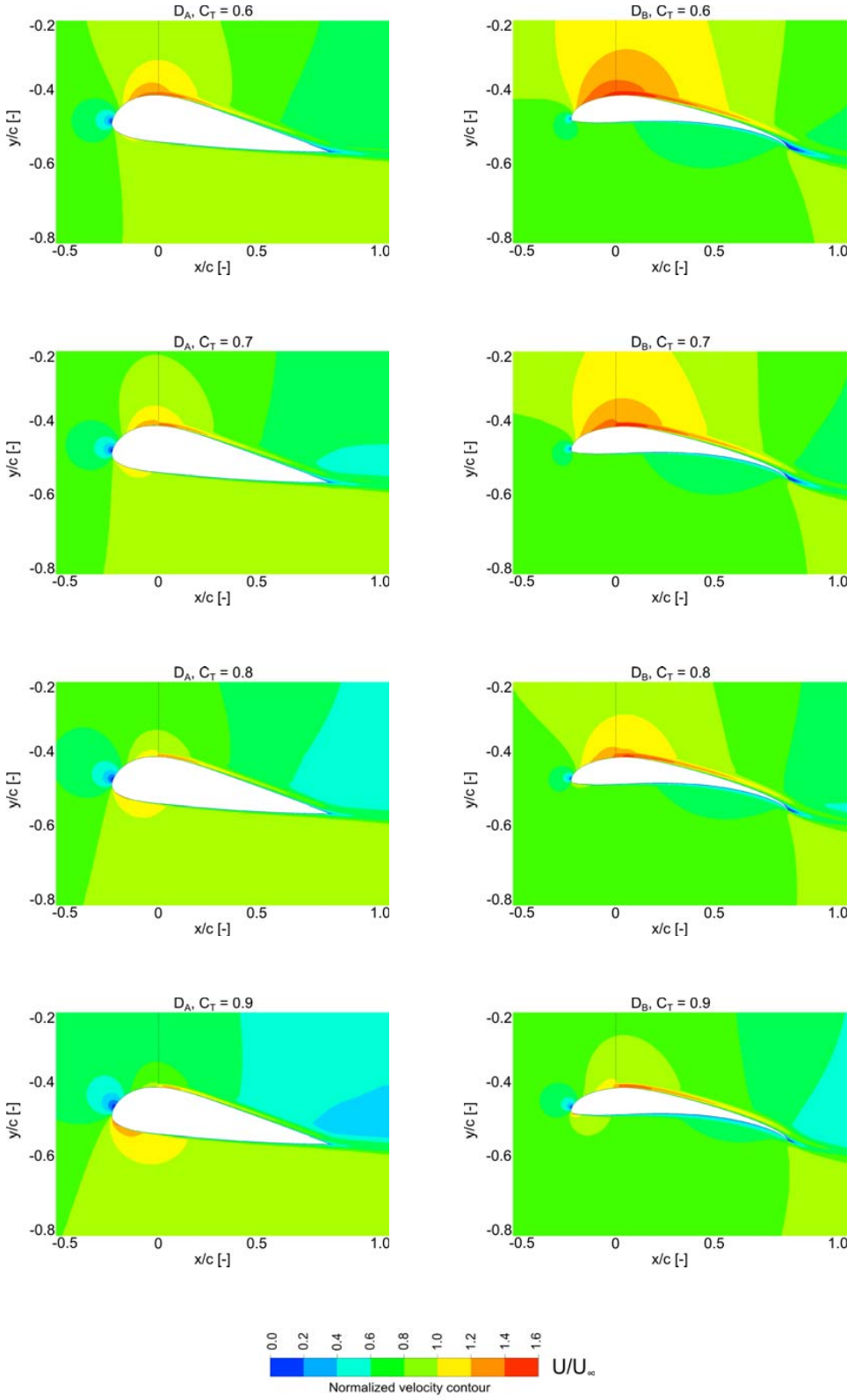

Figure 7. Normalized velocity contours for the duct-actuator model with duct D_A (left) and duct D_B (right). The results are depicted for $C_T = 0.6$, 0.7, 0.8 and 0.9; top to bottom.

References

[1] Foreman, K. M., Gilbert B., and Oman R. "Diffuser augmentation of wind turbines." Solar Energy 20.4 (1978): 305-311.
[2] Vries, O. de. "Fluid dynamic aspects of wind energy conversion." AGARD No.243 (France), 1979.
[3] Igra, Ozer."Research and development for shrouded wind turbines." Energy Conversion and Management 21.1 (1981): 13-48.
[4] Gilbert, B. L., and Foreman. K. M. "Experiments with a diffuser-augmented model wind turbine." Journal of Energy Resources Technology 105.1 (1983): 46-53.
[5] Abe, K., Nishida, M., Sakurai, A., Ohya, Y., Kihara, H., Wada, E., and Sato, K. "Experimental and numerical investigations of flow fields behind a small wind turbine with a flanged diffuser." Journal of Wind Engineering and Industrial Aerodynamics 93.12 (2005): 951-970.
[6] Toshimitsu, K., Nishikawa, K., Haruki, W., Oono, S., Takao, M., and Ohya, Y. "PIV measurements of flows around the wind turbines with a flanged-diffuser shroud." Journal of Thermal Science 17.4 (2008): 375-380.
[7] Van Bussel, G. J. W. "The science of making more torque from wind: Diffuser experiments and theory revisited." Journal of Physics: Conference Series. Vol. 75. No. 1. IOP Publishing, 2007.
[8] Werle, Michael J., and Walter M. Presz. "Ducted wind/water turbines and propellers revisited." Journal of Propulsion and Power 24.5 (2008): 1146-1150.
[9] Khamlaj, Tariq Abdulsalam, and Markus Peer Rumpfkeil. "Theoretical Analysis of Shrouded Horizontal Axis Wind Turbines." Energies 10.1 (2017): 38.
[10] Hjort, S and Larsen, H. "A multi-element diffuser augmented wind turbine." Energies 7.5 (2014): 3256-3281.
[11] Bontempo, Rodolfo, and Marcello Manna. "Effects of duct cross section camber and thickness on the performance of ducted propulsion systems for aeronautical applications." International Journal of Aerospace Engineering (2016).
[12] De Oliveira, G., R. B. Pereira, D. Ragni, F. Avallone, and G. J. W. van Bussel. "How does the presence of a body affect the performance of an actuator disk?." Journal of Physics: Conference Series. Vol. 753. No. 2. IOP Publishing, 2016.
[13] Dighe, V. V., F. Avallone., J. Tang and G. J. W. van Bussel "Effects of Gurney Flaps on the Performance of Diffuser Augmented Wind Turbine." 35th Wind Energy Symposium. 2017.
[14] Dighe, V. V., F. Avallone., G. de Oliveira and G. J. W. van Bussel. "On the effects of the shape of the duct for ducted wind turbines." 2018 Wind Energy Symposium. 2018.
[15] Dighe, V. V., F. Avallone and G. J. W. van Bussel. "Computational study of diffuser augmented wind turbine using actuator disc force method." International Journal of Computational Methods and Experimental Measurements 4.4 (2016): 522-531.